Journal of Modern Technology and Engineering
Vol.6, No.2, 2021, pp.89-103

Jomard Publishing

A MEDIUM-SIZED NANOCLUSTERS Au_{38}: A NUMERICAL FINITE-DIFFERENCE METHOD WITH DFTB APPROACH

K. Vishwanathan*

Faculty of Natural Sciences and Technology, University of Saarland, 66123 Saarbrücken, Germany

Abstract. We present a vibrational spectrum analysis of Au_{38} cluster, with energy (-4.95 eV/atom) having a group symmetry C_1. We have carried out DFTB calculation by using the numerical finite-difference method and extracted the required force constants. Our calculations have a good agreement with the experimental results, that is, a thermodynamically very stable structure can not be crystalline, but having a high probability of amorphus. The lowest energy geometrical structures are being confirmed by comparison (of the nuclei coordination numbers) of the different axis of rotations at a standard orientation of crystal shape. Moreover, we have accurately predicted the vibrational frequency range from 1.62 to 298.53 cm^{-1} at $\Delta E = 0$. Significantly, the spectrum has shown 10 sets of double state degeneracy and the rest of the 88 spectrum's are having independent single state degeneracy. Amazingly, at NVM 101, 102 that gives a pair of degeneracy {238.54, 238.89} cm^{-1} that has occurred within the range of Mid Infrared MIR, IR-C 3330-200 cm^{-1}. Nevertheless, our investigation has revealed that the vibrational spectrum strongly depends upon the size, shape, and structure, as well as, stretching and bending vibrations of the atoms.

Keywords: Gold Atomic Clusters, Density-Functional Tight-Binding (DFTB) approach, Finite-Difference Method, Force Constants (FCs) and Vibrational Spectrum.

Corresponding author: K. Vishwanathan, Faculty of Natural Sciences and Technology, University of Saarland, 66123 Saarbrücken, Germany, Tel.: + 49-0151-63119680, e-mail: *vishwa_nathan_7@yahoo.com*

Received: 23 April 2021; Revised: 16 July 2021; Accepted: 5 August 2021; Published: 31 August 2021.

1 Introduction

Dedicated to Honorable Prof. Dr. Rudolph Arthur Marcus (born July 21, 1923) on the occasion of his 98th birthday, he is a Canadian-born chemist who received the 1992 Nobel Prize in Chemistry "for his contributions to the theory of electron transfer reactions in chemical systems".
Marcus theory, named after him, provides a thermodynamic and kinetic framework for describing one electron outer-sphere electron transfer. He is a professor at Caltech, Nanyang Technological University, Singapore and a member of the International Academy of Quantum Molecular Science.
As for me, it was the highest privilege that we met each other at the international Conference on TACC, Gyeongju, S. Korea, 2004 which has inspired me to lay down my life into Scientific Career.

In general, nanoclusters are interesting because their physical, optical and electronic characteristics are strongly size dependent. Often changing the size by only one atom can significantly alter the physical chemical properties of the system (Wu et al., 2016), for that reasons, many new periodic tables can thus be envisioned classifying differently-sized clusters of the same material as new elements. Potential applications are enormous, ranging from devices in nano-electronics and nano-optics (Andres et al., 1996) to applications in medicine and materials.

Gold colloids not only having some practical application recently, but also, have been used for centuries to stain glass which has been even used for the study of direct electrochemistry of proteins (Kamat, 2002). The main reasons are, gold is a soft metal and is usually alloyed to give it more strength. In addition to that gold is a good conductor of heat and electricity, and is unaffected by air and most reagents. Noble-metal (Cu, Ag, and Au) clusters have attracted much attention in scientific and technological fields because of their thermodynamic, electronic, optical and catalytic properties in nano-materials (Li et al., 2016; Zhang et al., 2019).

The vibrational properties play a major role in structural stability (Garzón & Posada-Amarillas, 1996; Bravo-Pérez et al., 1999a,b; Sauceda et al., 2012, 2013a,b; Sauceda & Garzón, 2015; Dugan & Erkoç, 2008). The structural determination of metal nanoparticles of their vibrational (phonon) density of states have been calculated by Sauceda & Garzón (2015). Specific heat capacity is an important thermodynamic property and is directly related to the structural stability, identification and energy of substances. Most recently, Sauceda et al. (2013a) calculated vibrational properties and specific heat of core-shell Ag-Au icosahedral nanoparticles.

Most recently, many researchers have observed that, beyond Au_{25}^{-1}, the low-symmetry core-shell structures dominate the low-energy clusters, and the hollow-cage structures are unlikely to exist in larger size due to the strong relativistic effects (Shao et al., 2010). Zhang et al. (2019), worked on the lowest-energy geometrical and electronic structures of Cu_{38}^{-1} clusters which are investigated by density functional calculations combined with a genetic algorithm based on a many body semi-empirical interatomic potential, the traditional FCC-truncated Octahedron (OH) and an incomplete-Mackay icosahedron (IMI) are recognized as the two lowest energy structures (energetically degenerate isomers) but with different electronic structures: a semiconductor-type with the energy-gap of 0.356 eV for the IMI and a metallic-type with negligible gap for the OH, which is in good agreement with the experimental results. The electron affinity and ionization potential of Cu_{38}^{-1} are also discussed and compared with the observations of the ultraviolet photoelectron spectroscopy experiments. The dynamical isomerization of the OH-like and IMI-like structures of Cu_{38}^{-1} is revealed to dominate the premelting stage through the investigation by the molecular dynamics annealing simulations.

Above all, recent theoretical study of Au_{38}^{-1}, Zhao et al. (2013) also suggest a spindle-like structure of Au_{38}^{-1}, which contains a tetrahedral core. The structures of gold clusters in the size regime between 36 and 54 atoms have not been confirmed experimentally. In search for such structural information, the questions are: Is the tetrahedral core so stable that it can be retained in Au clusters beyond the size Au_{36}^{-1}? If it is, at what size of Au cluster would the tetrahedral core transform to a different core? Also, what would the next core structure look like? To answer some of these questions and to understand the structural growth pattern of medium-sized Au clusters, they have performed a global structure search of low-energy clusters of Au_{36}^{-1} to Au_{38}^{-1} by using the basin-hopping (BH) global optimization method (Wales & Scheraga, 1999) combined with DFT calculations. The most stable structures are identified by comparing the experimental PES spectra with the computed electronic density of states of all lowest-lying isomers (Bulusu et al., 2006; Huang et al., 2009; Li et al., 2003).

In this study, we focus on the vibrational properties of gold clusters with sizes Au_{38} atoms. Some general information about global minima gold structures which have been calculated by the work Dong & Springborg (2007); Warnke (2007). The structures were found through a so called *genetic algorithm* (GA) in combination with *Density Functional Tight-Binding* (DFTB) energy calculations and a *steepest descent* algorithm permitting a local total energy minimization. Nevertheless, peculiarly, in our case, we use our numerical finite-difference approach Dvornikov (2004) along with density functional tight-binding (DFTB) method and extracted the vibrational spectrums. Overall, for a better understanding and to visualize, the detailed information is discussed in the results and discussion section.

2 Theoretical and Computational Procedure

At first, the DFTB (Porezag et al., 1995; Seifert & Schmidt, 1992; Seifert et al., 1996) is based on the density functional theory of Hohenberg and Kohn in the formulation of Kohn and Sham. In addition, the Kohn-Sham orbitals $\psi_i(\mathbf{r})$ of the system of interest are expanded in terms of atom-centered basis functions $\{\phi_m(\mathbf{r})\}$,

$$\psi_i(\mathbf{r}) = \sum_m c_{im}\phi_m(\mathbf{r}), \quad m = j. \tag{1}$$

While so far the variational parameters have been the real-space grid representations of the pseudo wave functions, it will now be the set of coefficients c_{im}. Index m describes the atom, where ϕ_m is centered and it is angular as well as radially dependant. The ϕ_m is determined by self-consistent DFT calculations on isolated atoms using large Slater-type basis sets.

In calculating the orbital energies, we need the Hamilton matrix elements and the overlap matrix elements. The above formula gives the secular equations

$$\sum_m c_{im}(H_{mn} - \epsilon_i S_{mn}) = 0. \tag{2}$$

Here, c_{im}'s are expansion coefficients, ϵ_i is for the single-particle energies (or where ϵ_i are the Kohn-Sham eigenvalues of the neutral), and the matrix elements of Hamiltonian H_{mn} and the overlap matrix elements S_{mn} are defined as

$$H_{mn} = \langle \phi_m \mid \hat{H} \mid \phi_n \rangle, \quad S_{mn} = \langle \phi_m \mid \phi_n \rangle. \tag{3}$$

They depend on the atomic positions and on a well-guessed density $\rho(\mathbf{r})$. By solving the Kohn-Sham equations in an effective one particle potential, the Hamiltonian $\hat{H}$ is defined as

$$\hat{H}\psi_i(\mathbf{r}) = \epsilon_i\psi_i(\mathbf{r}), \quad \hat{H} = \hat{T} + V_{eff}(\mathbf{r}). \tag{4}$$

To calculate the Hamiltonian matrix, the effective potential V_{eff} has to be approximated. Here, $\hat{T}$ being the kinetic-energy operator $\sum(\hat{T} = -\frac{1}{2}\nabla^2)$ and $V_{eff}(\mathbf{r})$ being the effective Kohn-Sham potential, which is approximated as a simple superposition of the potentials of the neutral atoms,

$$V_{eff}(\mathbf{r}) = \sum_j V_j^0(\mid \mathbf{r} - \mathbf{R}_j \mid). \tag{5}$$

V_j^0 is the Kohn-Sham potential of a neutral atom, $\mathbf{r}_j = \mathbf{r} - \mathbf{R}_j$ is an atomic position, and $\mathbf{R}_j$ being the coordinates of the j-th atom.

Finally, the short-range interactions can be approximated by simple pair potentials, and the total energy of the compound of interest relative to that of the isolated atoms is then written as,

$$\begin{aligned} E_{tot} \simeq \sum_i \epsilon_i - \sum_j \sum_{m_j}^{occ} \epsilon_{jm_j} + \frac{1}{2}\sum_{j\neq j'} U_{jj'}(\mid \mathbf{R}_j - \mathbf{R}_{j'} \mid), \\ \epsilon_B \equiv \sum_i^{occ} \epsilon_i - \sum_j \sum_{m_j}^{occ} \epsilon_{jm_j} \end{aligned} \tag{6}$$

Here, the majority of the binding energy (ϵ_B) is contained in the difference between the single-particle energies ϵ_i of the system of interest and the single-particle energies ϵ_{jm_j} of the isolated atoms (atom index j, orbital index m_j), $U_{jj'}(\mid \mathbf{R}_j - \mathbf{R}_{j'} \mid)$ is determined as the difference between ϵ_B and ϵ_B^{SCF} for diatomic molecules (with E_B^{SCF} being the total energy from parameter-free density-functional calculations). In the present study, only the $5d$ and $6s$ electrons of the gold

atoms are explicitly included, whereas the rest are treated within a frozen-core approximation (Porezag et al., 1995; Seifert et al., 1996; Seifert, 2007).

3 The Hessian Matrix

In short, this method is described as follows: The Hessian matrix is represented in an orthonormal basis consisting of the five or six eigenvectors of the Hessian matrix which span its kernel and of $(3N-5)\,or\,(3N-6)$ arbitrarily chosen mutually orthonormal basis vectors, which are orthogonal to the kernel-eigenvectors. When represented in this basis, the Hessian should be partially diagonal. The diagonal part is now cut away and the remaining Hessian is diagonalized to reveal the eigenfrequencies of the clusters normal modes.

The Hessian matrix is the matrix of second derivatives of the energy with respect to geometry which is quite sensitive to its geometry. Energy second derivatives are evaluated numerically. The mass-weighted Hessian matrix is obtained by numerical differentiation of the analytical first derivatives, calculated at geometries obtained by incrementing in turn each of the $3N$ nuclear coordinates by a small amount ds with respect to the equilibrium geometry. The introduction of the Hessian matrix and its diagonalization ultimately leads to the eigen-frequencies of the system and its eigenvectors, describing the harmonic motion of the clusters atoms. In order to obtain the matrix elements H_{ij} of the Hessian matrix which are needed if one wishes to investigate the clusters thermodynamic properties and one should obtain the derivatives of potential energy surface (**PES**) (Warnke, 2007; Press et al., 2007).

3.1 Cutting off the Kernel

The Hessian matrix $\mathbf{H}$ is symmetric by Schwarz' theorem. The Kernel of $\mathbf{H}$ consists of all vectors which describe pure translational and rotational motion of the center of mass of the molecule, leaving its internal structure untouched. This is the eigenspace of $\mathbf{H}$ which is associated to the eigenvalue 0. As we have 5 for linear 6 for non-linear degrees of freedom corresponding to such translations and rotations, $dim(Ker(\mathbf{H})) = 5\,or\,6$. We denote the five or six Hessian eigenvectors associated to the Kernel $\mathbf{k}^{(1)},...,\mathbf{k}^{(5\,or\,6)} \in \Re^{3N}$. The remaining $(3N-5)\,or\,(3N-6)$ Hessian eigenvectors denoted by $\mathbf{n}^{(1)},...,\mathbf{n}^{(3N-5)\,or\,(3N-6)} \in \Re^{3N}$, form a basis of the $(3N-5)\,or\,(3N-6)$ dimensional configuration space, in which the molecular structure may be described uniquely without any reference to the position or orientation of the molecule relative to an inertial system.

In our method, we apply the Gram-Schmidt theorem, to set up an orthonormal basis for $\Re^{3N}$. The basis of the Kernel consisting of the five or six hessian eigenvectors $\mathbf{k}^{(1)},...,\mathbf{k}^{(5\,or\,6)}$ can easily be found, they are the orthonormalized translations and rotations of the structure. Now, we simply use $\mathbf{k}^{(1)},...,\mathbf{k}^{(5\,or\,6)}$ as the first five or six basis vectors for an orthonormal basis of $\Re^{3N}$ denoted $\mathbf{C}$. The remaining $(3N-5)\,or\,(3N-6)$ basis vectors of $\mathbf{C}$ are the arbitrarily chosen mutually orthonormal vectors $\mathbf{c}^{(1)},...,\mathbf{c}^{(3N-5)\,or\,(3N-6)}$, which have to satisfy $\langle \mathbf{k}^{(i)} \mid \mathbf{c}^{(j)} \rangle = 0$ for any possible combination of i and j.

By construction, the basis vectors $\mathbf{c}^{(1)},...,\mathbf{c}^{(3N-5)\,or\,(3N-6)}$ of basis $\mathbf{C}$ form a basis of the $(3N-5)\,or\,(3N-6)$ dimensional configuration space which is the subspace of $\Re^{3N}$ without translations and rotations. Consequently, the Hessian $\mathbf{H}$, which is of $rank(\mathbf{H}) = (3N-5)\,or\,(3N-6)$ can be fully represented in the configuration space, the normal modes $\mathbf{n}$ do not contain any components of the basis $\mathbf{k}^{(1)},...,\mathbf{k}^{(5\,or\,6)}$ of the kernel of the Hessian. Thus, the normal modes $\mathbf{n} \in \Re^{3N}$, satisfying the condition $\langle \mathbf{n}^{(i)} \mid \mathbf{n}^{(j)} \rangle = \delta_{ij}$ can be expanded in the basis $\mathbf{c}^{(1)},...,\mathbf{c}^{(3N-5)\,or\,(3N-6)}$ of the configuration space and they will still be orthonormal.

Now, let us represent $\mathbf{H}$ in the basis $\mathbf{C}$. Let $\mathbf{U} \in \mathbf{M}(\Re^{3N} \times \Re^{3N})$ be the matrix consisting of the column vectors of $\mathbf{C}$, *i.e.,*

$$U = \begin{pmatrix} \mathbf{k}_1^{(1)} & \mathbf{k}_1^{(2)} & ... & \mathbf{k}_1^{(5\,or\,6)} & \mathbf{c}_1^{(1)} & ... & \mathbf{c}_1^{(3N-5)\,or\,(3N-6)} \\ \mathbf{k}_2^{(1)} & \mathbf{k}_2^{(2)} & ... & \mathbf{k}_2^{(5\,or\,6)} & \mathbf{c}_2^{(1)} & ... & \mathbf{c}_2^{(3N-5)\,or\,(3N-6)} \\ \mathbf{k}_3^{(1)} & \mathbf{k}_3^{(2)} & ... & \mathbf{k}_3^{(5\,or\,6)} & \mathbf{c}_3^{(1)} & ... & \mathbf{c}_3^{(3N-5)\,or\,(3N-6)} \\ & & . & & . & & . \\ & & . & & . & & . \\ & & . & & . & & . \\ \mathbf{k}_{3N}^{(1)} & \mathbf{k}_{3N}^{(2)} & ... & \mathbf{k}_{3N}^{(5\,or\,6)} & \mathbf{c}_{3N}^{(1)} & ... & \mathbf{c}_{3N}^{(3N-5)\,or\,(3N-6)} \end{pmatrix} \tag{7}$$

Since $\mathbf{U}$ is a unitary transformation, the complex-conjugate of $\mathbf{U}$ is equal to its inverse, *i.e.,* $\mathbf{U}^*=\mathbf{U}^{-1}$ and thus the sought representation $\mathbf{H}'$ of $\mathbf{H}$ in the new basis $\mathbf{C}$ is found by calculating $\mathbf{U}^*\mathbf{H}\mathbf{U} = \mathbf{H}'$

Since the first five or six vectors $\mathbf{k}^{(1)}, ..., \mathbf{k}^{(5\,or\,6)}$ of the basis $\mathbf{C}$ are the eigenvectors corresponding to translation and rotation, the first five or six lines and columns of the representation $\mathbf{H}'$ of $\mathbf{H}$ in this basis should be diagonal and the eigenvalues which are the $\mathbf{H}'$'s diagonal elements should be equal to 0.

Diagonalization of the non-diagonal submatrix $\mathbf{H}'' \in \mathbf{M}(\Re^{(3N-5)\,or\,(3N-6)})$ which is the representation of the Hessian in the basis $\mathbf{c}^{(1)}, ..., \mathbf{c}^{(3N-5)\,or\,(3N-6)}$ of the configuration space, yields its eigenvectors, *i.e.,* the $(3N-5)\,or\,(3N-6)$ normal modes $\mathbf{n}'^{(1)}, ..., \mathbf{n}'^{(3N-5)\,or\,(3N-6)} \in \Re^{(3N-5)\,or\,(3N-6)}$. The diagonal elements are the sought eigenvalues, the eigenfrequencies of the normal modes which are needed for the calculation of thermodynamic properties.

First, we set up an orthonormal basis which allows to separate $\Re^{3N}$ into its $(3N-5)\,or\,(3N-6)$-dimensional configuration subspace and the complementary five or six dimensional subspace which makes reference to absolute position and orientation of the molecule. The latter is not needed for the description of the molecule's structure and the normal modes. Second, we represent the Hessian in this basis and cut away the part belonging to the five or six-dimensional complementary space, before the new Hessian $\mathbf{H}'' \in \mathbf{M}(\Re^{(3N-5)\,or\,(3N-6)} \times \Re^{(3N-5)\,or\,(3N-6)})$ finally is diagonalized to reveal its eigenvalues and -vectors.

For quite all systems, results obtained in both ways, with the above method and without it were compared. The results are very close to each other. The numerically optimized structures are almost exact and/or the Hessian matrix changes very little around the minimum and the numerical error can be ignored, using an appropriate method. Applying the new method in our further calculations, we were able to find positive semidefinite Hessian matrices $\mathbf{H}''$ for all structures.

3.2 Calculation of the Numerical Force Constants (FCs)

A re-optimized structure of the force constants (FCs) could be extracted from the already optimized structure (Dong & Springborg, 2007) as the following, the force(s) expressions were obtained by derivation of the energy expression (or) from the expression of energy, the forces can be easily calculated by derivation. Here, the Force(s) $\mathbf{F}_j$ that act on the j-th atom of the system can be calculated applying the Hellmann-Feynman theorem (Hellmann, 1937; Feynman, 1939), so the forces are given as,

$$\mathbf{F}_j = -\nabla_j E_{tot} = -\frac{\partial E_{tot}}{\partial \mathbf{R}_j} \tag{8}$$

These are all identical to 0 (within numerical accuracy) for the optimized structure (Dong & Springborg, 2007). Interatomic forces can easily be derived from an exact calculation of the

gradients of the total energy at the considered atoms site, finally, the forces acting on an atom at $\mathbf{R}_j$ are obtained as follows:

$$\mathbf{F}_j = \sum_{i}^{occ} \sum_{m,n} c_{im} c_{in} \left(-\frac{\partial H_{mn}}{\partial \mathbf{R}_j} + \epsilon_i \frac{\partial S_{mn}}{\partial \mathbf{R}_j} \right) + \frac{1}{2} \sum_{j \neq j'} \frac{\partial}{\partial \mathbf{R}_j} U_{jj'}(\mid \mathbf{R}_j - \mathbf{R}_{j'} \mid) \tag{9}$$

To extract the required force constants (FCs), the numerical first-order derivatives of the forces used instead of the numerical-second-order derivatives of the total energy. In principle there is no difference, but numerically the approach of using the forces is more accurate. A finite difference formula has been introduced as following (Dvornikov, 2004),

$$\begin{aligned} \frac{\partial^2 E_{tot}}{\partial \mathbf{R}_{i\alpha} \partial \mathbf{R}_{j\beta}} &= \frac{\partial}{\partial \mathbf{R}_{i\alpha}} \left[\frac{\partial E_{tot}}{\partial \mathbf{R}_{j\beta}} \right] = \frac{\partial}{\partial \mathbf{R}_{i\alpha}} (\text{-}\mathbf{F}_{j\beta}) = \frac{\partial}{\partial \mathbf{R}_{j\beta}} (\text{-}\mathbf{F}_{i\alpha}) \\ \frac{\partial^2 E_{tot}}{\partial \mathbf{R}_{i\alpha} \partial \mathbf{R}_{j\beta}} &= \frac{1}{2} \frac{1}{ds} \left[\frac{\partial}{\partial \mathbf{R}_{i\alpha}} (\text{-}\mathbf{F}_{j\beta}) + \frac{\partial}{\partial \mathbf{R}_{j\beta}} (\text{-}\mathbf{F}_{i\alpha}) \right] \end{aligned} \tag{10}$$

In principle, there is no difference, but numerically the approach of using the forces is more accurate, for homonuclear case, M represents the atomic mass, for convenience eqn. (10) can be written as

$$\frac{1}{M} \frac{\partial^2 E_{tot}}{\partial \mathbf{R}_{i\alpha} \partial \mathbf{R}_{j\beta}} = \frac{1}{M} \frac{1}{2ds} \left[\frac{\partial}{\partial \mathbf{R}_{i\alpha}} (\text{-}\mathbf{F}_{j\beta}) + \frac{\partial}{\partial \mathbf{R}_{j\beta}} (\text{-}\mathbf{F}_{i\alpha}) \right] \tag{11}$$

In total we end up with $(3N \times 3N)$ values $\frac{\partial^2 E}{\partial \mathbf{R}_{i\alpha} \partial \mathbf{R}_{j\beta}}$. The complete list of these force constants (FCs) is called the Hessian $\mathbf{H}_{ij}$, which is a $(3N \times 3N)$ matrix. Here, i is the component of (x, y or z) of the force on the j'th atom, so we get $3N$. The ds is nothing but a differentiation step-size.

4 Results and Discussion

4.1 The optimized structure of the cluster Au_{38}

We present a vibrational spectrum analysis of re-optimized Au_{38} cluster, having energy (-4.95 eV/atom) with a group symmetry C_1 at $\Delta E = 0$. Initially, the structures were found through a so called *genetic algorithm* (GA) in combination with *Density Functional Tight-Binding* (DFTB) energy calculations and a *steepest descent* algorithm permitting a local total energy minimization (Dong & Springborg, 2007).

In our case, we have accurately predicted the vibrational frequencies of the clusters which are very strongly depend on the size, the structure and the shape of the clusters, as well as, mainly the spectrum ranges are influenced by the stretching and the bending mode vibrations of the atoms that happens due to the changes on the bond length fluctuations on the PES of equilibrium coordinates for a small step-size $ds = \pm 0.01$ a.u.. The detailed information can be found below.

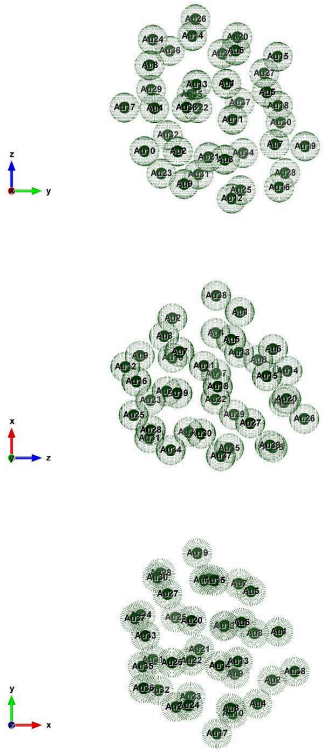

Figure 1: Au_{38} (C_1); Style (Wireframe): View along the a-axis, b-axis and c-axis (from top to bottom) at $\Delta E = 0$.

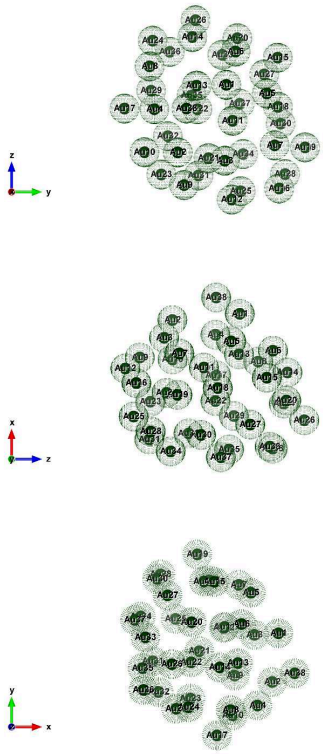

Figure 2: Au_{38} (C_1) ; Style (Wireframe): View along the a*-axis, b*-axis and c*-axis (from top to bottom) at $\Delta E = 0$.

4.2 The vibrational frequency (ω_i) range of the cluster Au_{38} at $\Delta E = 0$

Table 1 shows that the low (at the least) and the high (at the most) frequency range of cluster Au_{38}. The lowest and the highest frequency range in between 1.62 cm^{-1} to 298.53 cm^{-1}.

Firstly, the cluster has some low frequencies (ω_{min}) in between 1.62-9.81 cm^{-1}, that is only for the very first 8 NVM, which comes even below the scale of Far Infrared FIR, IR-C 200-10 cm^{-1}.

Secondly, for the 9-92 NVM, the frequency ranges are occurred in between 11.98-199.43 cm^{-1}, which comes within the range of Far Infrared FIR, IR-C 200-10 cm^{-1}.

Thirdly, for the rest of the 93-108 NVM, are having the maximum high frequencies, which are ((ω_i) - 205.14-298.53 cm^{-1}) falling within the range of Mid Infrared MIR, IR-C 3330-200 cm^{-1}.

Table 1: Calculated vibrational frequency (ω_i) range of the re-optimized gold atomic cluster, Au_{38} at $\Delta E = 0$. Normal modes and the corresponding vibrational frequencies (ω_i) are in cm^{-1}.

NVM (3N-6)	ω_i cm^{-1}	NVM (3N-6)	ω_i cm^{-1}	NVM (3N-6)	ω_i cm^{-1}	NVM (3N-6)	ω_i cm^{-1}
1	1.62	28	31.77	55	74.41	82	163.80
2	2.85	29	34.41	56	80.07	83	164.35
3	3.51	30	35.20	57	82.44	84	169.29
4	6.58	31	35.40	58	86.02	85	173.54
5	7.13	32	36.75	59	86.95	86	179.60
6	7.67	33	37.54	60	90.02	87	184.56
7	8.49	34	38.99	61	91.61	88	187.06
8	9.81	35	40.34	62	94.83	89	192.05
9	11.98	36	42.83	63	100.22	90	194.80
10	12.47	37	44.17	64	101.26	91	197.09
11	13.19	38	47.30	65	103.00	92	199.43
12	14.02	39	47.89	66	105.42	93	205.14
13	14.58	40	48.79	67	108.33	94	208.83
14	15.21	41	50.40	68	111.57	95	211.31
15	16.31	42	51.64	69	115.52	96	215.72
16	16.80	43	54.34	70	121.19	97	220.88
17	18.54	44	54.84	71	124.43	98	223.94
18	18.97	45	56.43	72	128.45	99	224.58
19	20.05	46	58.32	73	130.20	100	231.38
20	21.66	47	61.07	74	136.19	101	238.54
21	22.39	48	62.63	75	137.73	102	238.89
22	24.21	49	64.68	76	143.49	103	249.08
23	25.96	50	67.74	77	148.10	104	254.35
24	27.46	51	69.47	78	150.45	105	260.13
25	27.76	52	71.31	79	151.95	106	262.69
26	28.62	53	72.20	80	158.18	107	276.44
27	29.72	54	73.05	81	160.72	108	298.53

4.3 The double and the single state degeneracy of the cluster Au_{38} at $\Delta E = 0$

First of all, the vibrational spectra of eigenvalues were found in the region between 1.62 and 298.53 cm^{-1}. Mainly, we have observed the most of the eigenvalues (88) are non-degenerate (single state) vibrations. Moreover, 20 out of 108 (NVM of (3N-6)) has 10 pairs of double-fold

degeneracy (see Table 1). This gives a very strong confirmation of the energy can be observed and be released with the same amount that corresponds to a certain local bong length rearrangements. Very interestingly, at NVM 101, 102 that gives a pair of degeneracy {238.54, 238.89 } cm^{-1} that has occurred within the range of Mid Infrared MIR, IR-C 3330-200 cm^{-1}. Surely, such kind of spectrum could be highly possible to observe in the experimental calculations. The other extreme case, NVM 5, 6 gives a pair of degeneracy {7.13, 7.67} cm^{-1} which has occurred even below the scale of Far Infrared FIR, IR-C 200-10 cm^{-1}, the most probably this could be silent in the experimental case. Finally, the consecutive pairs are: NVM 15, 16 $\rightarrow$ {16.31, 16.80} cm^{-1} and NVM 17, 18 $\rightarrow$ {18.54, 18.97} cm^{-1}, which has occurred within the scale of Far Infrared FIR, IR-C 200-10 cm^{-1}, it reveals openly and gives a confirmation of four-edged core-level atoms are moving equally having with the same bond lengths on the clusters, additionally, this also can be observable in the experimental way of calculations.

Mainly, on the clusters, the degree of degeneracy is being released due to the bond length fluctuation of the symmetric as well as anti-symmetric move of the atoms. Additionally, for understanding and describing the atomic interactions in the cluster (Wales, 2013; Ballard et al., 2015; Martiniani et al., 2014; Mandelshtam et al., 2006; Sharapov & Mandelshtam, 2007; Sharapov et al., 2007), one must have the basic knowledge of, if the energy absorbed when bond breaks, at the same time, the energy released when bond forms. When increase the bond length then bond strength will become weaker but if we bring closer the bond length to each other, as a result, the bond strength will become stronger. We can observe attraction with a shared electrons as well as repulsion due to nuclei and electron shell. In addition to that due to the degree of degeneracy [which are being composed by] that gives a deep interpretation about the elliptical motion but that could be a single motion.

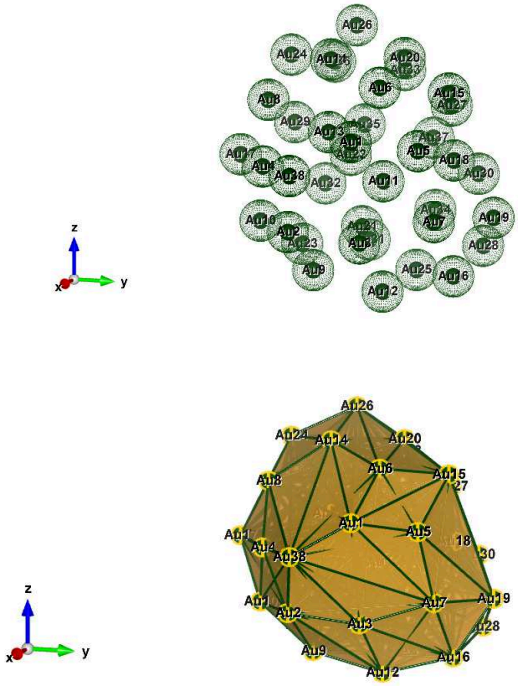

Figure 3: Au_{38} (C_1); Style (Wireframe, Polyhedral): The lowest energy geometrical structures of Au_{38} cluster. Standard orientation of crystal shape at $\Delta E = 0$.

In total, when two atoms come very close, the force between them is always repulsive, because the electrons stay outside and the nuclei repel each other. Unless both atoms are ions of the same charge (e.g., both negative) the forces between atoms is always attractive at large internuclear

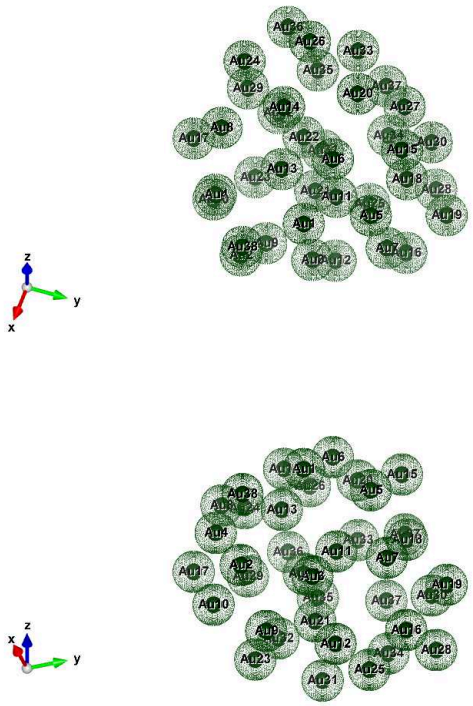

Figure 4: Au_{38} (C_1); Style (Wireframe): Rotate around the x axis (upward direction [above] and downward direction [below]) at $\Delta E = 0$.

distances r. Since the force is repulsive at small r, and attractive at small r, there is a distance at which the force is zero. This is the equilibrium distance at which the atoms prefer to stay. The interaction energy is the potential energy between the atoms. It is negative if the atoms are bound and positive if they can move away from each other. The interaction energy is the integral of the force over the separation distance, so these two quantities are directly related. The interaction energy is a minimum at the equilibrium position. This value of the energy is called the bond energy, and is the energy needed to separate completely to infinity (the work that needs to be done to overcome the attractive force.) The strongest the bond energy, the hardest is to move the atoms, for instance the hardest it is to melt the solid, or to evaporate its atoms. As a result, this makes a complete structure for those collection of the atoms.

4.4 Structural view of the shapeless structures

In one case, from the Figs. 1, 2; we are looking down the direct space a, b, or c axis and in the other case we are looking down the reciprocal space a*, b* and c* axes. Since the axis of Cartesian coordinates does not have any changes, because it is not a crystal structure.

Fig 3. clearly shows the standard orientation of crystal shape of $Au_{38}(C_1)$ cluster at $\Delta E = 0$ (the lowest energy geometrical structure). Nevertheless, to see the perspective view, we have plotted with a two different style (Wireframe, Polyhedral).

Above all, from the Figs. 4, 5 and 6 we are able to see the minute detailed information of all different kinds of rotations that help us to visualize as well as to understand the orientation of the structures. Example: the structures are being rotated around the X-axis, the Y-axis and the Z-axis [See the number of faces, vertices and edges]. Over all, in the perspective view the shell-like structures are found. It is suggested that the ability of gold to form strong binding in low-coordinated systems is the reason for the occurrence of shell-like structures. This cluster is composed of two shells surrounding a central atom.

Shao (2014) reported a joint experimental and theoretical study of the structural evolution

of medium-sized gold clusters. They found that the most stable structures of Au_{36}^{-1} to Au_{38}^{-1} exhibit core-shell type structures all with a highly robust tetrahedral four-atom core. All of their three clusters are observed to possess two coexisting isomers in the cluster beam. The appearance of a fragment of the face centered cubic (FCC) bulk gold, that is, the pyramidal Au_{20}^{-1}, at the size of Au_{38}^{-1} implies that the cluster-to-bulk transformation starts to emerge at the medium size range. It is expected that larger pyramidal like intermediates may emerge in later medium-to large-sized Au clusters beyond Au_{38}^{-1}.

Surely, our numerical calculations performed within this study confirms the theoretical and the experimental results: The most stable configuration of the cluster is not crystalline but with a high probability this cluster is a shapeless. This cluster was composed of two shells surrounding a central atom. Furthermore, a shell structure should not be considered as a kind of ordering in the context of small nanoparticles. Even the random arrangement of gold atoms, used as starting condition for some of the calculations, shows such a shell structure. We conclude that, the highest probability of the lowest energy structure can be amorphous (as non-crystalline), which is an excellent agreement with the conclusion of the known results (Shao, 2014; Doye, 1998; Huang, 2008; Wang L.M. & Wang L.S., 2012).

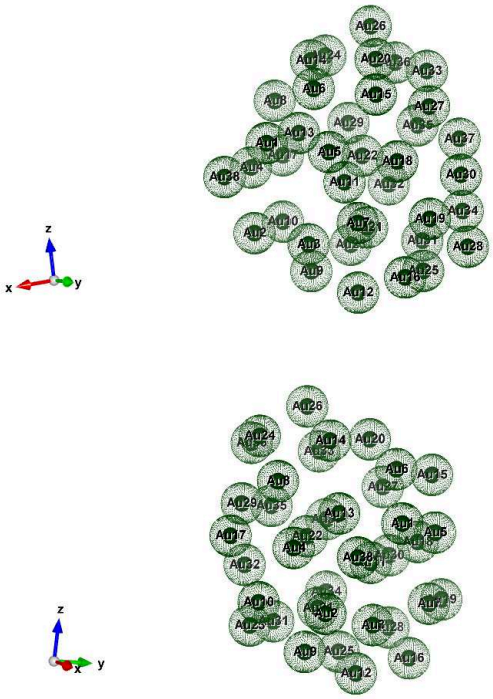

Figure 5: Au_{38} (C_1); Style (Wireframe): Rotate around the y axis (LHS direction [above] and RHS direction [below]) at $\Delta E = 0$.

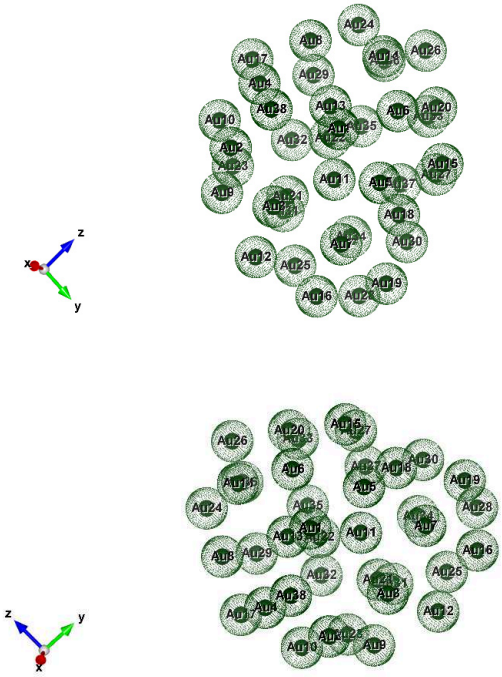

Figure 6: Au_{38} (C_1); Style (Wireframe): Rotate around the z axis (clockwise (CW) direction [above] and anti-clockwise (ACW) direction [below]) at $\Delta E = 0$.

5 Conclusion

We have calculated the vibrational frequency (at $\Delta E = 0$) of a medium-sized nanoclusters Au_{38}, the shell-like structure (of course, they are part of the family of so-called full-shell clusters), by using a numerical finite-difference method with DFTB approach. Last but not least, our present study gives an additional support to the prediction of the existence of shapeless (due to the absence of symmetry) stable structures on the metal clusters. The appearance of such structures will always depend on the range of the n-body interactions which are responsible for the metallic cohesion in those systems. Above all, our investigation has revealed that the vibrational spectrum strongly depends upon the size, the shape, and the structure of the atomic cluster.

6 Funding

Initially, the main part of this work was supported by the German Research Council (DFG) through project Sp 439/23-1. We gratefully acknowledge their very generous support.

References

Andres, R.P., Bein, T., Dorogi, M., Feng, S., Henderson, J.I., Kubiak, C.P., ... & Reifenberger, R. (1996). "Coulomb staircase" at room temperature in a self-assembled molecular nanostructure. *Science, 272*(5266), 1323-1326.

Ballard, A.J., Martiniani, S., Stevenson, J.D., Somani S. & Wales, D.J. (2015). Wiley Interdisciplinary Reviews: *Computational Molecular Science.,* 5, 273-289.

Bravo-Pérez, G., Garzón, I.L., & Novaro, O. (1999a). Ab initio study of small gold clusters. *Journal of Molecular Structure: THEOCHEM, 493*(1-3), 225-231.

Bravo-Pérez, G., Garzón, I.L., & Novaro, O. (1999b). Non-additive effects in small gold clusters. *Chemical physics letters, 313*(3-4), 655-664.

Bulusu, S., Li, X., Wang, L.S., & Zeng, X.C. (2006). Evidence of hollow golden cages. *Proceedings of the National Academy of Sciences, 103*(22), 8326-8330.

Dong, Y., Springborg, M. (2007). Global structure optimization study on Au_{2-20}. *The European Physical Journal D, 43*(1), 15-18.

Doye, J.P., Wales, D.J. (1998). Global minima for transition metal clusters described by Sutton-Chen potentials. *New Journal of Chemistry, 22*(7), 733-744.

Dugan, N., Erkoç, S. (2008). Stability analysis of graphene nanoribbons by molecular dynamics simulations. *Physica Status Solidi (B), 245*(4), 695-700.

Dvornikov, M. (2004). Formulae of numerical differentiation. Preprint, arXiv:math.NA/0306092v3.

Feynman, R.P. (1939). Forces in molecules. *Phys. Rev.*, 56.

Garzón, I.L., Posada-Amarillas, A. (1996). Structural and vibrational analysis of amorphous Au_{55} clusters. *Physical Review B, 54*(16), 11796.

Hellmann, H. (1937). Einführung in die Quantenchemie Deuticke.

Huang, W., Bulusu, S., Pal, R., Zeng, X.C., & Wang, L.S. (2009). CO chemisorption on the surfaces of the golden cages. *The Journal of chemical physics, 131*(23), 234-305.

Huang, W., Ji, M., Dong, C.D., Gu, X., Wang, L.M., Gong, X.G., & Wang, L.S. (2008). Relativistic effects and the unique low-symmetry structures of gold nanoclusters. *ACS Nano, 2*(5), 897-904.

Kamat P.V. (2002). Photophysical, Photochemical and Photocatalytic Aspects of Metal Nanoparticles. *J. Phys. Chem. B.*, 106, 7729-7744, doi: 10.1021/jp0209289.

Li, J., Liu, Y., Zhang, J., Liang, X. & Duan, H. Density functional theory study of the adsorption of hydrogen atoms on Cu_2X (X = 3d) clusters. *Chem. Phys. Lett.*, 651, 137-143, https://doi.org/10.1016/j.cplett.2016.03.035

Li, J., Li, X., Zhai, H.J., & Wang, L.S. (2003). Au_{20}: a tetrahedral cluster. *Science*, *299*(5608), 864-867.

Mandelshtam, V.A., Frantsuzov, P.A., & Calvo, F. (2006). Structural transitions and melting in LJ_{74-78} Lennard-Jones clusters from adaptive exchange Monte Carlo simulations. *The Journal of Physical Chemistry A, 110*(16), 5326-5332.

Martiniani, S., Stevenson, J.D., Wales, D.J., & Frenkel, D. (2014). Superposition enhanced nested sampling. *Physical Review X, 4*(3), 031034.

Porezag, D., Frauenheim, T., Köhler, T., Seifert, G., & Kaschner, R. (1995). Construction of tight-binding-like potentials on the basis of density-functional theory: Application to carbon. *Physical Review B, 51*(19), 12947.

Press, W.H., Teukolsky, S.A., Vetterling, W.T., & Flannery, B.P. (2007). *Numerical Recipes with Source Code CD-ROM 3rd Edition: The Art of Scientific Computing.* Cambridge University Press.

Sauceda, H.E., Garzón, I.L. (2015). Structural determination of metal nanoparticles from their vibrational (phonon) density of states. *The Journal of Physical Chemistry C, 119*(20), 10876-10880.

Sauceda, H.E., Mongin, D., Maioli, P., Crut, A., Pellarin, M., Del Fatti, N., ... & Garzón, I.L. (2012). Vibrational properties of metal nanoparticles: Atomistic simulation and comparison with time-resolved investigation. *The Journal of Physical Chemistry C, 116*(47), 25147-25156.

Sauceda, H.E., Pelayo, J.J., Salazar, F., Pérez, L.A., & Garzón, I.L. (2013a). Vibrational spectrum, caloric curve, low-temperature heat capacity, and Debye temperature of sodium clusters: the Na_{139^+} case. *The Journal of Physical Chemistry C, 117*(21), 11393-11398.

Sauceda, H.E., Salazar, F., Pérez, L.A., & Garzón, I.L. (2013b). Size and shape dependence of the vibrational spectrum and low-temperature specific heat of Au nanoparticles. *The Journal of Physical Chemistry C, 117*(47), 25160-25168.

Seifert, G. (2007). Tight-binding density functional theory: an approximate Kohn- Sham DFT scheme. *The Journal of Physical Chemistry A, 111*(26), 5609-5613.

Seifert, G., Porezag, D., & Frauenheim, T. (1996). Calculations of molecules, clusters, and solids with a simplified LCAO-DFT-LDA scheme. *International Journal of Quantum Chemistry, 58*(2), 185-192.

Seifert, G., Schmidt, R. (1992). Molecular dynamics and trajectory calculations: the application of an LCAO-LDA scheme for simulatins of cluster-cluster collisions. *New Journal of Chemistry, 16*(12), 1145-1147.

Shao, N., Huang, W., Mei, W.N., Wang, L.S., Wu, Q., & Zeng, X.C. (2014). Structural evolution of medium-sized gold clusters Au_{n^-} $(n = 36, 37, 38)$: appearance of bulk-like face centered cubic fragment. *The Journal of Physical Chemistry C, 118*(13), 6887-6892.

Shao, N., Huang, W., Gao, Y., Wang, L.M., Li, X., Wang, L.S., & Zeng, X.C. (2010). Probing the Structural Evolution of Medium-Sized Gold Clusters: Au_{n^-} $(n = 27 - 35)$. *Journal of the American Chemical Society, 132*(18), 6596-6605.

Sharapov, V.A., Mandelshtam, V.A. (2007). Solid-solid structural transformations in Lennard-Jones clusters: Accurate simulations versus the harmonic superposition approximation. *The Journal of Physical Chemistry A, 111*(41), 10284-10291.

Sharapov, V.A., Meluzzi, D., & Mandelshtam, V.A. (2007). Low-temperature structural transitions: Circumventing the broken-ergodicity problem. P*hysical Review Letters, 98*(10), 105701.

Wales, D.J. (2013). Surveying a complex potential energy landscape: Overcoming broken ergodicity using basin-sampling. *Chemical Physics Letters,* 584, 1-9.

Wales, D.J., Scheraga, H.A. (1999). Global optimization of clusters, crystals, and biomolecules. S*cience, 285*(5432), 1368-1372.

Wang, L.M., Wang, L.S. (2012). Probing the electronic properties and structural evolution of anionic gold clusters in the gas phase. *Nanoscale, 4*(14), 4038-4053.

Warnke, I. (2007). Heat Capacities of Metal Clusters. Diploma Thesis (Research Assistant and Diploma Research), Saarland University.

Wu, L., Fang, W., & Chen, X. (2016). The photoluminescence mechanism of ultra-small gold clusters. *Physical Chemistry Chemical Physics, 18*(26), 17320-17325.

Zhang, C., Duan, H., Lv, X., Cao, B., Abliz, A., Wu, Z., & Long, M. (2019). Static and dynamical isomerization of Cu_{38} cluster. *Scientific reports, 9*(1), 1-9.

Zhao, L.X., Zhang, M., Feng, X.J., Zhang, H.Y., Zhang, W.L., & Luo, Y.H. (2013). Stuffed Cage Structures and Properties of Neutral and Charged Au_{38} Nanocluster. *Journal of Cluster Science, 24*(1), 123-131.